ACS Macro Letters

pubs.acs.org/macroletters Letter

Fast and Integral Nano-Surface-Coating of Various Fiber Materials via Interfacial Polymerization

Aqiang Wang, Shoujian Gao, Yuzhang Zhu,* and Jian Jin*

Cite This: ACS Macro Lett. 2023, 12, 93−100 Read Online

ACCESS | Metrics & More | Article Recommendations | Supporting Information

ABSTRACT: Surface coating is essential and critical to endow fiber materials with various functions for broad applications. However, it is still a great challenge to achieve a fast, fully covered, and robust surface coating on multiple fibers. In this work, a nanoscale surface coating with superior stability was rapidly and integrally formed on various fiber materials (such as Nylon mesh, nonwoven fabrics, and stainless-steel mesh) by highly reactive interfacial polymerization (IP) between polyethylenimine (PEI) and trimesoyl chloride (TMC). The resulting polyamide (PA) layer with an ultrathin thickness of tens of nanometers wholly and uniformly covered the surface of each fiber of the constituent material. Due to the synergistic effect of the PA layer with inherent robustness and the fully covered structure between the outer PA layer and the inner fiber, the nanosurface-coating exhibited outstanding mechanical stability, good acid resistance, and excellent organic solvent resistance. The functional modification of the nanosurface-coating can be easily carried out by using the abundant carboxyl groups in the PA layer. By introducing sulfobetaine zwitterionic copolymers via either "grafting from" or "grafting to" methods, the surfaces presented prominent underwater antioil-adhesion property and exceptional protein adhesion resistance. The surface coating based on IP process opens up an avenue in the field of surface modification. It is expected to offer a generally feasible strategy for the fabrication of fiber materials with robust and multifunctional coatings.

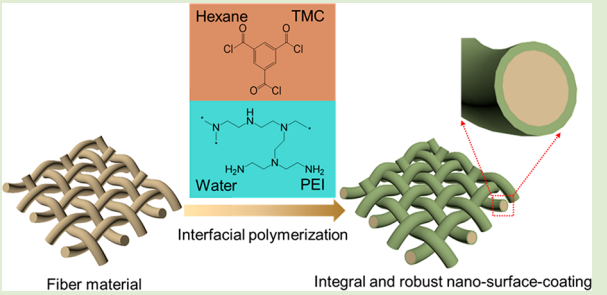

In the past decades, fiber materials have attracted increasing focus in the fields of membrane separation,[1−3] biomedical engineering,[4−6] sensors and actuators,[7−9] energy storage and conversion,[10,11] and wearable electronics[12−14] due to the merits of large specific surface area, tunable pore size, high porosity, high mechanical strength, good flexibility and connectivity, and so on.[15−18] However, the surface of raw fiber materials, whether from natural fibers such as cotton or synthetic fibers such as polyester, must be functionally modified in order to achieve more diversified functions and better properties.[15,19,20] Through blending functional materials with matrix in the process of fiber spinning, composite fiber materials can be endowed with specific properties.[21] However, these functional materials are prone to unevenly distribute in the matrix owing to poor compatibility.[22,23] Besides, the blending method is not suitable for the modification of the fibers composed of metal, glass, and most natural fibers. Generally, post-treatment strategies, including chemical modification and physical coating, are widely used.[24−26] Chemical modification is an effective strategy to endow fibers with various functions by introducing a chemical reaction between the modifier and the fiber.[27−30] However, it usually requires abundant reaction sites on the surface of fiber materials. Insufficient reaction sites will result in incomplete coverage of the modified layer and reduce the modification effect. Grafting polymerization is an effective method to increase the content of functional components in case of relatively few reaction sites. However, grafting polymerization usually needs harsh operating condition, tedious operation processes, and long preparation time.[22,31,32]

As a simple and convenient strategy, fibers with various functions through a series of physical coating processes, including dip coating,[33−35] spin coating,[36−38] layer-by-layer assembly,[39,40] and chemical vapor deposition,[41,42] have been well developed. However, as a matter of fact, it is still a challenge to obtain a uniform and complete coating with thickness at the nanoscale on a fiber material. In the process of physical coating, the concentration, viscosity, preparation time, operation speed, and/or equipment parameters must be accurately adjusted and strictly controlled. In some physical coating, the fiber materials are required to have specific surface groups or charges.[43] In addition, due to the weak noncovalent interactions with the fibers, the physical coating is easy to fall off and be damaged.[44,45] Recently, mussel-inspired coating has

Received: October 26, 2022
Accepted: December 29, 2022
Published: January 3, 2023

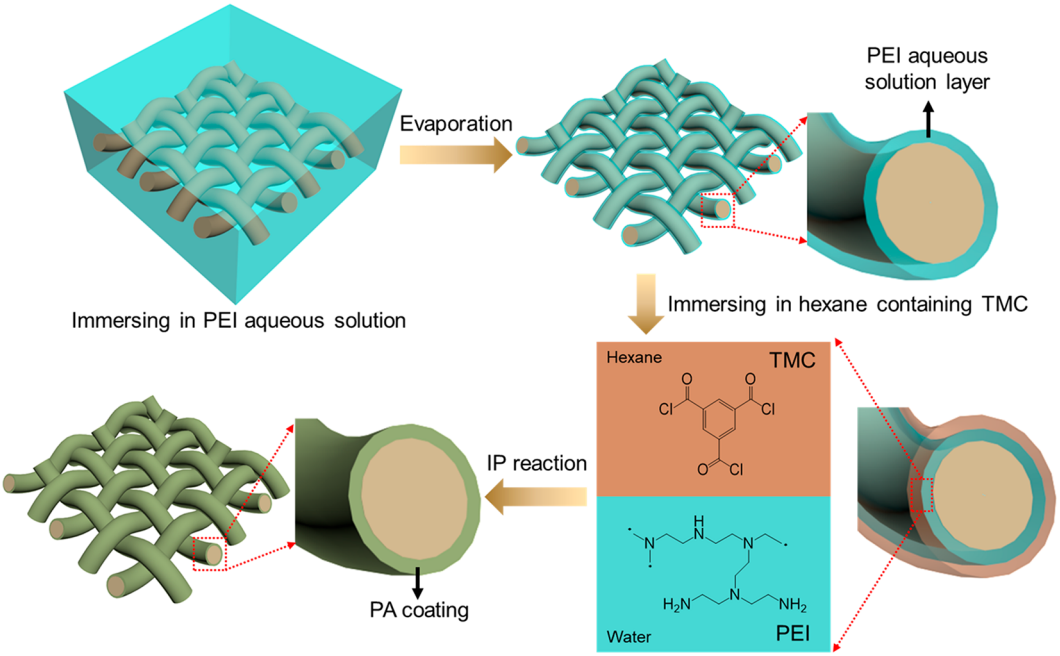

Figure 1. Schematic showing the fast and integral formation of the PA coating on a fiber material via the IP reaction of PEI in aqueous solution and TMC in hexane.

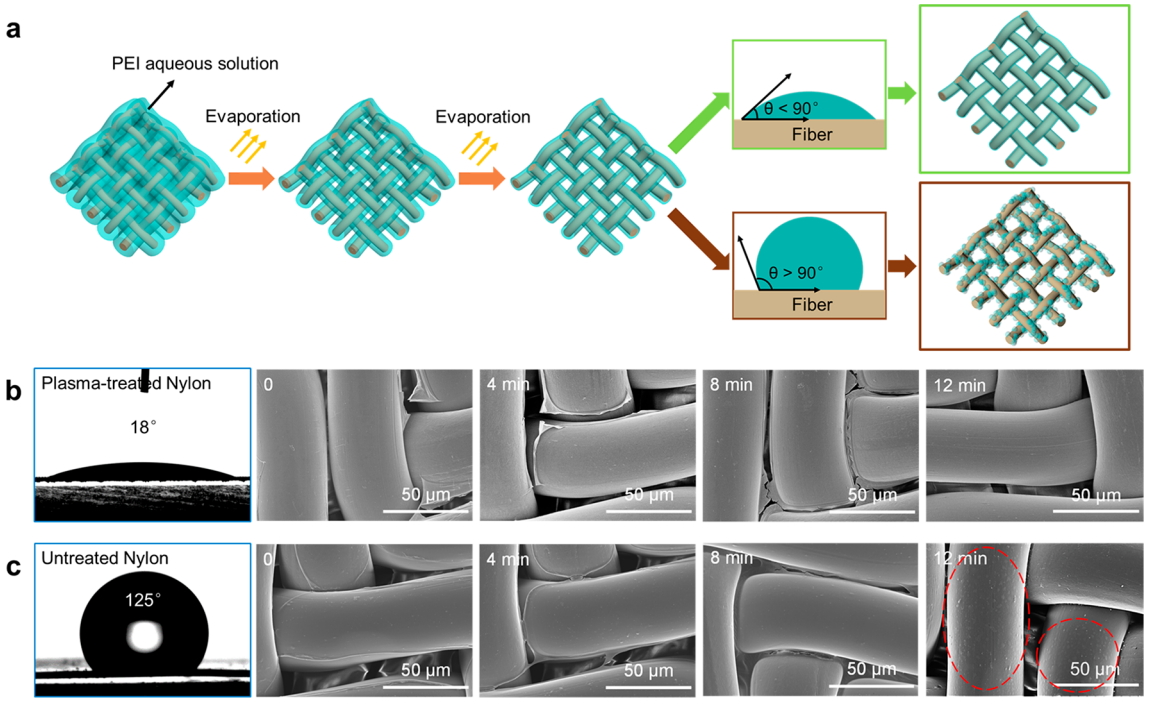

Figure 2. (a) Schematic showing the evaporation process to remove the excess PEI aqueous solution and form the thin solution layer on hydrophilic and hydrophobic fiber surfaces. Water CAs of the (b) plasma-treated Nylon mesh and (c) untreated Nylon mesh, as well as SEM images of PA coatings fabricated on these Nylon meshes when evaporating the PEI solution for different time.

attracted great attention and been extensively studied.[46−49] Although the mussel-inspired coatings can easily adhere on various substrates based on multiple interactions, they are highly likely to be formed by the accumulation of nanoparticles and difficult to form a uniform and complete coating on the nanoscale.[50,51] Developing a facile and universal strategy for constructing a nanoscale, uniform and robust surface coating is thus highly desired and of great significance to further promote the development and application of fiber materials.

In this work, we report a new surface coating strategy on various fibers by utilizing liquid/liquid interfacial polymerization (IP). The IP process is a general and industrialized strategy widely used in the preparation of reverse osmosis membrane and nanofiltration membrane, where a homogeneous and continuous ultrathin polyamide (PA) layer with a thickness of tens of nanometers can be rapidly formed on a porous support by the cross-linking reaction between amine in aqueous solution and acyl chloride in hexane.[52−56] Herein, the

https://doi.org/10.1021/acsmacrolett.2c00631
ACS Macro Lett. 2023, 12, 93−100

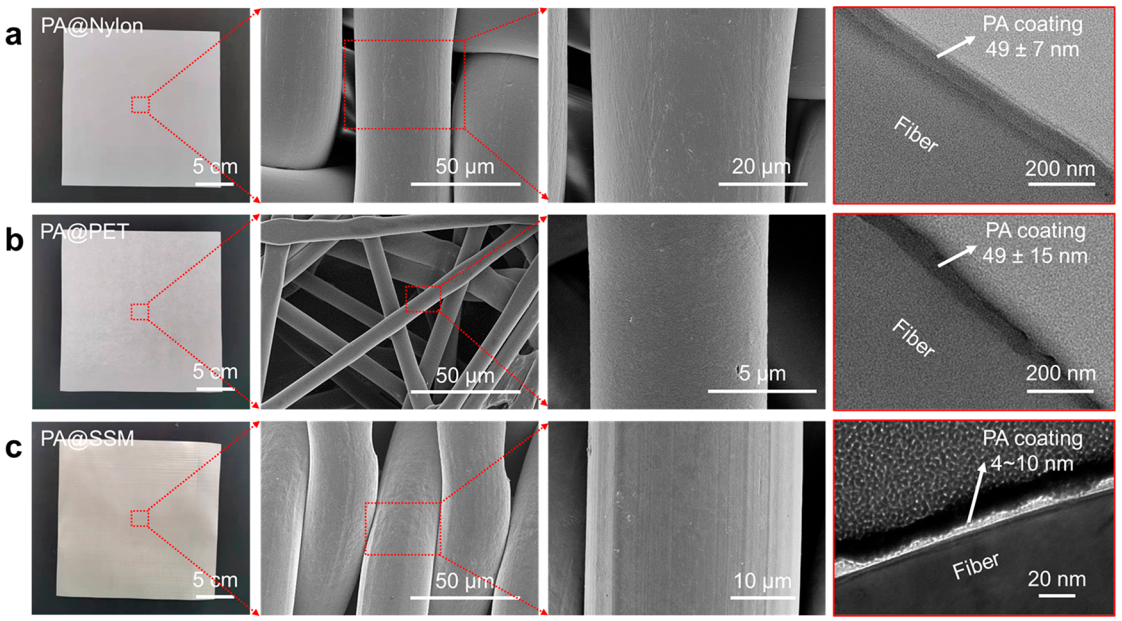

Figure 3. Optical, SEM, and TEM images of the (a) PA@Nylon, (b) PA@PET, and (c) PA@SSM. Cross-sectional TEM images in the red frames show the structures and thicknesses of the corresponding PA coatings.

IP process was first used to modify fiber materials. Through the IP reaction of polyethylenimine (PEI) and trimesoyl chloride (TMC), we successfully constructed a surface coating that can be tightly wrapped on the surface of fibers composed of various materials and with a diameter of microns or even coarser. Due to the inherent self-limitation property of the IP process, the obtained surface coating could be well controlled in tens of nanometers and is extremely uniform with 100% coverage. The surface coating shows excellent mechanical stability and plays the role of physical isolation, which can effectively protect the internal fibers from the damage of the external environment. The PA coating contains a large number of residual amine and carboxyl groups derived from the hydrolysis of unreacted acryloyl chloride groups.[57−59] These groups can be used as reaction sites for further functional modification of fibers. We grafted zwitterions onto the coating surface to endow the fiber material with superhydrophilic and excellent antifouling properties. Our work opens up a new avenue in the field of surface modification and is expected to offer a generally feasible strategy for the fabrication of fiber materials with robust and multifunctional coatings.

To construct the IP-based surface coating, a fiber material pretreated to be hydrophilic was alternatively soaked in an aqueous solution containing PEI and a hexane solution containing TMC, as schematically illustrated in Figure 1 (see detail in the Experimental Section, SI). In this work, a Nylon mesh was pretreated by plasma and showed a water contact angle (CA) of 18° (Figure S1a). A polyethylene terephthalate (PET) nonwoven fabric was pretreated by alkali and showed a water CA of 58°. A stainless-steel mesh (SSM) was precleaned and showed a water CA of 89°. The pretreated fiber material was completely immersed in the PEI aqueous solution for 3 min and then placed under an ambient condition to allow the excess PEI aqueous solution to evaporate. By controlling the ambient temperature and humidity as well as accurately adjusting the evaporation time, a thin and uniform PEI aqueous solution layer wrapped the fibers was achieved. When the TMC hexane solution was introduced onto the fiber material, IP reaction occurred rapidly at the interface of the two solutions, forming a PA layer coating each fiber. As a direct evidence for the formation of PA coatings, the water CA on Nylon, PET, and SSM mesh exhibited obvious change after the reaction (Figure S1).

It is well-known that the PA layer grows along the interface between the aqueous solution and organic solution during the IP reaction, and the geometric shape of the interface primarily determines the one of PA layer. Therefore, the key of fabricating the integral and uniform PA coatings on the fibers lies in the formation of a thin and continuous PEI aqueous solution layer on the fiber surfaces. As illustrated in Figure 2a, when fabricating the PA coating on a hydrophilic fiber material, we can gradually remove the excess PEI solution via evaporation to form the required PEI solution layer to obtain the uniform PA coating surrounding the fibers after the IP process. However, for hydrophobic fiber material, the PEI solution cannot form the required PEI solution layer after the same evaporation, but will shrink to aqueous droplets on the fibers. As a consequence, the randomly distributed PA flecks will be obtained after the same IP process. As shown in Figure 2b,c, a series of PA coatings are fabricated on the hydrophilic and hydrophobic Nylon meshes with evaporating the PEI solution for different time. For a plasma-treated hydrophilic Nylon mesh (water CA: 18°), when the IP process is implemented on the mesh without evaporating the PEI solution, the excess PEI solution reacts with the TMC solution and generates an incomplete PA layer on the upper surface of the whole mesh (Figure 2b). When evaporating the PEI solution for 4 or 8 min, the excess PEI solution on the mesh is partly removed. The PA layer trends to be generated on the fiber surfaces after the IP process, but several PA slices are also generated on the fiber edges. When evaporating the PEI solution for 12 min, the excess PEI solution is totally removed, a thin and continuous PEI aqueous solution layer is formed on the fiber surface. Eventually, a uniform PA coating is generated surrounding the fibers. For an untreated hydrophobic Nylon mesh (water CA: 125°), when evaporating the PEI solution for

https://doi.org/10.1021/acsmacrolett.2c00631
ACS Macro Lett. 2023, 12, 93−100

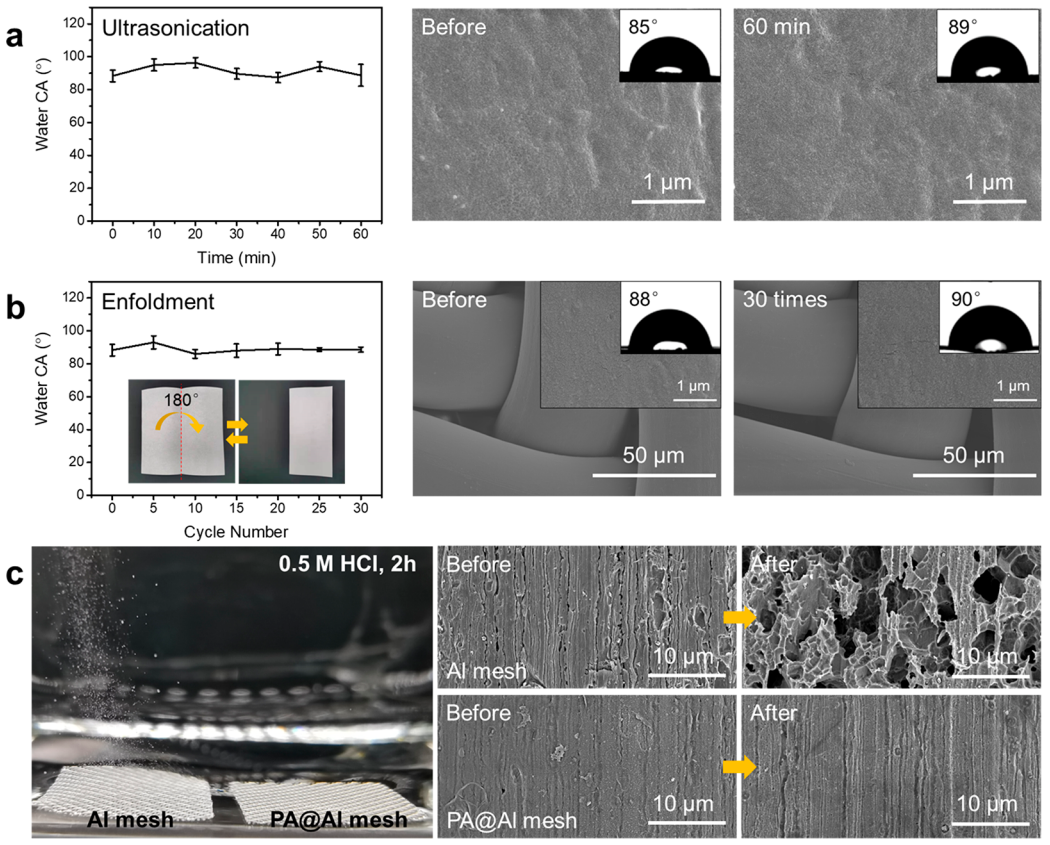

Figure 4. (a) Water CA variation of the PA@Nylon along with the ultrasonication time and the corresponding SEM images of the PA@Nylon before and after the ultrasonication for 60 min. (b) Water CA variation of the PA@Nylon along with the enfoldment cycles and the corresponding SEM images of the PA@Nylon before and after the enfoldment for 30 cycles. (c) Optical image and SEM images showing the uncoated Al mesh and PA@Al mesh in a 0.5 M HCl solution for 2 h.

0, 4, and 8 min, similar PA layers to those generated on the hydrophilic Nylon mesh are successively obtained (Figure 2c). When evaporating the PEI solution for 12 min, some PA flecks rather than a uniform PA coating are generated on the fibers after the same IP process (Figures 2c and S2). This is because some PEI solution droplets rather than a solution layer are left on the hydrophobic Nylon fibers after the evaporation. For other hydrophilic fiber materials like alkali-treated PET nonwoven fabric (water CA: 58°) and precleaned SSM mesh (water CA: 89°), we get the consistent result, as shown in Figure S3, and obtain the uniform PA coating with an evaporation time of 16 min. Therefore, the construction of the uniform PA coating is dependent on both the hydrophilicity of the fiber materials and the appropriate evaporation time to remove the excess PEI solution.

Figure 3 shows the structures of the PA-layer coated fiber materials, including the Nylon mesh, PET nonwoven fabric, and stainless-steel mesh, which are denoted as PA@Nylon, PA@PET, and PA@SSM, respectively. The square PA@Nylon, PA@PET, and PA@SSM with side lengths of around 20 cm was successfully fabricated and exhibited homogeneous surface morphologies. From the scanning electron microscope (SEM) images and high-resolution cross-sectional transmission electron microscope (TEM) images of the PA@Nylon, PA@PET, and PA@SSM, the obtained PA coating layers are all integrally coated on the surfaces of the fibers with no visible defects even on the junctions of two neighboring fibers. The PA coatings are all very uniform and dense. The thicknesses of the PA coatings are 49 ± 7, 49 ± 15, and 4−10 nm corresponding to PA@Nylon, PA@PET, and PA@SSM, respectively. In addition, the TEM images of the cross section of a single fiber in the PA@PET were also observed at a small magnifica-tion (Figure S4), further confirming the existence of uniform and integral PA coating. These results demonstrate that our surface coating strategy is generally feasible to construct ultrathin and uniform PA coatings on various fiber materials, regardless of material type, fiber diameter, and pore structure.

Surface morphology and chemical composition of the PA coatings constructed on different fiber materials were investigated in detail. As shown in the high-resolution SEM images (Figure S5), the PA coatings on the PA@Nylon, PA@PET and PA@SSM are all continuous and defect-free, with nearly 100% coverage on the fiber surfaces. The N 1s peaks in the X-ray photoelectron spectroscopy (XPS) spectra prove the formation of the PA coatings on these fiber materials (Figure S6a). On the other hand, the percentages of C, N, and O elements are almost the same for the PA@Nylon, PA@PET, and PA@SSM (Figure S6b), indicating that the PA coatings have covered ∼100% of the fiber surfaces with nearly no fiber surfaces exposure. The chemical composition of the PA coatings was analyzed based on the binding energy of C- and O-related groups (Figure S7). The C 1s peak can be split into three peaks which are attributed to C−H/C-C bond at 284.5 eV, C−N bond at 285.8 eV and N−C═O/O−C═O bond at 287.8 eV, respectively. The O 1s peak can be split into two peaks which are attributed to N−C═O bond at 531.0 eV and O−C═O at 532.7 eV, respectively. By calculating the integral

https://doi.org/10.1021/acsmacrolett.2c00631
ACS Macro Lett. 2023, 12, 93−100

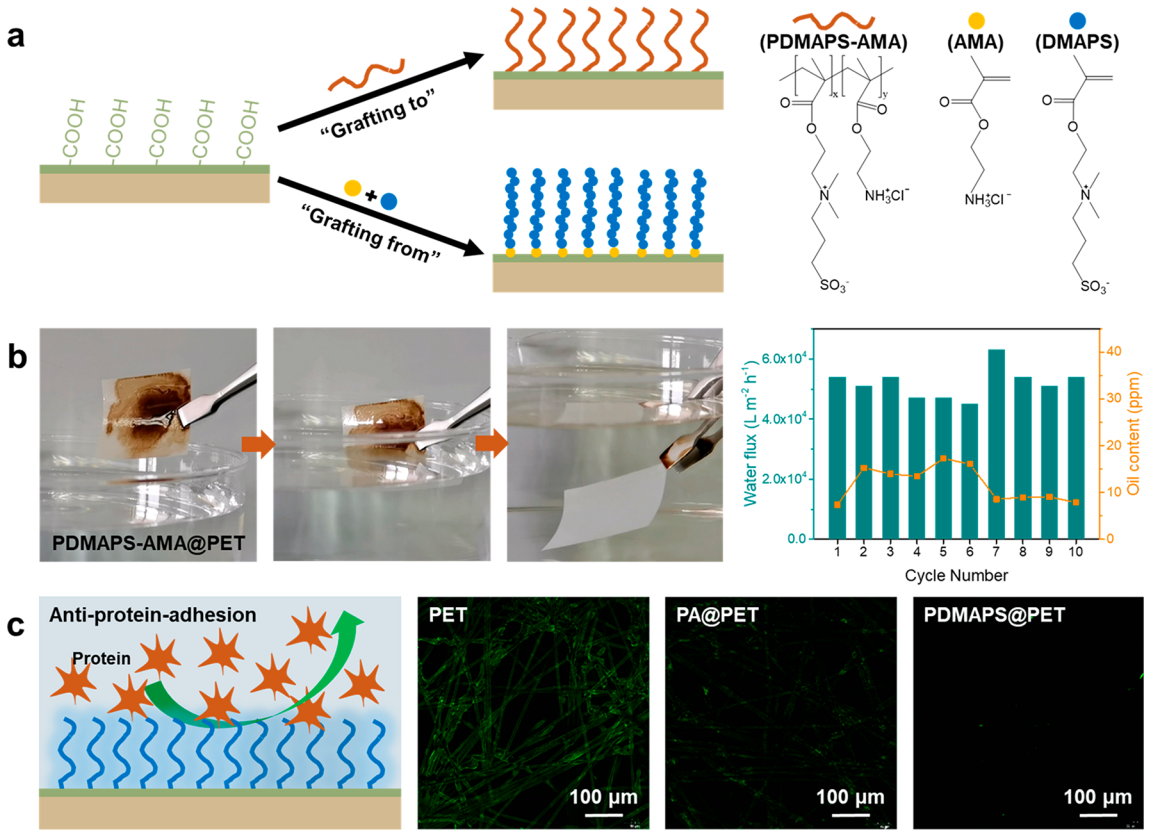

Figure 5. (a) Schematical illustrations of functional modifcation on the nanosurface-coating via either "grafting to" or "grafting from" methods. (b) Underwater anticrude-oil-adhesion property of PDMAPS-AMA@PET and its separation performance in the 10-cycle separation process for crude oil/water mixture. (c) A schematic showing antiprotein-adhesion process as well as confocal fluorescence microscopy images of the pristine PET, PA@PET, and PDMAPS@PET after being immersed in a FITC-BSA solution for 3 h.

areas of the split peaks, the percentages of corresponding chemical groups are summarized in Table S1. Among them, the percentages of O−C═O groups are 4.3%, 5.5%, and 3.8% for PA@Nylon, PA@PET, and PA@SSM, respectively. The carboxyl groups are derived from the hydrolysis of unreacted acryloyl chloride groups in TMC, and can provide reaction sites for further functionalization on the PA coating. The spatial distribution of elements in PA@PET and PA@SSM was also measured by the energy dispersive X-ray (EDX) imaging (Figure S8). Comparing the nearly same EDX maps of C and N in the PA@PET, it can be inferred that N is uniformly distributed on the PET fibers surfaces (Figure S8a). This result further demonstrates that the PA coating is perfectly covered the fibers of the PA@PET. Similarly spatial distribution of N element was also detected for the PA@SSM, suggesting the existence of perfect PA coatings as well (Figure S8b).

Stability is of great significance as for a surface coating. To investigate the mechanical stability of the PA coating, the tests of ultrasonication and enfoldment were carried out on a PA@Nylon (Figure 4). During the ultrasonication test with a power of 90 W for 60 min, the PA@Nylon shows stable water CAs of 92 ± 7° (Figure 4a). Meanwhile, the morphology of the PA@Nylon before and after the ultrasonication is unchanged, indicating that the PA coating is stably modified on the fibers without damage. During the enfoldment test in which the PA@Nylon is folded in half and then unfolded for 30 cycles, the PA@Nylon also exhibits stable with water CAs of 90 ± 4° (Figure 4b). No exfoliation phenomena of the PA coating occur after 30 enfoldment cycles. These results demonstrate the excellent mechanical stability of the PA coating on the fiber materials. The chemical stability of the PA coating was also evaluated by immersing the PA@Nylon in an acid solution (pH = 2), an alkali solution (pH = 12), acetone, and *N*,*N*-dimethylformamide (DMF), respectively, for 12 h. During the treatments of acid, acetone and DMF, the PA@Nylon maintains stable water CAs of 87 ± 6° (Figure S9a,c,d), as well as barely changed morphologies (Figure S10). It demonstrates the good stability and resistance of the PA coating to acid and organic solvents. During the treatment of alkali, the water CA of the PA@Nylon gradually decreases from 89° to 63° (Figure S9b), and some cracks appear on the PA coating (Figure S10). The weak stability of the PA coating in alkali is ascribed to the hydrolysis of the amide bond. To investigate the protective function of the PA coating, a PA layer coated aluminum (PA@Al) mesh and an uncoated Al mesh were both immersed in a 0.5 M HCl solution for 2 h. As shown in Figure 4c, plenty of H_2 bubbles are generated from the uncoated Al mesh, and the mesh surface is seriously corroded due to the reaction of Al and HCl. Whereas, no H_2 bubbles are generated from the PA@Al mesh, and the surface morphology of the PA@Al mesh is well maintained. It further demonstrates the 100% coverage and outstanding acid resistance of the PA coating.

The abundant carboxyl groups on the PA coating provide the reaction sites for further modification and construction of other functional surface coatings as shematically shown in (Figure 5a). Here we give two examples. One is the construction of the surface with underwater antioil-adhesion

https://doi.org/10.1021/acsmacrolett.2c00631
ACS Macro Lett. 2023, 12, 93−100

property by grafting a sulfobetaine zwitterionic copolymer on the PA coating via a "grafting to" method (Figure 5b). Figure S11 reveals the chemical structure of the zwitterionic copolymer, poly(3-((2-(methacryloyloxy)ethyl) (dimethyl)-ammonio)-1-propanesulfonate)-*co*-poly(2-aminoethyl methacrylate hydrochloride) (PDMAPS-AMA), which was synthesized via a free radical copolymerization. Under the catalysis of *N*-(3(dimethylamino)propyl)-*N*′-ethylcarbodiimide hydrochloride (EDC) and *N*-hydroxysuccinimide (NHS), the amino groups in the PDMAPS-AMA form covalent bonds with the carboxyl groups in the PA coating. The PDMAPS-AMA is thus grafted to the PA coating. The PA@Nylon, PA@PET, and PA@SSM modified by the PDMAPS-AMA are denoted as PDMAPS-AMA@Nylon, PDMAPS-AMA@PET, and PDMAPS-AMA@SSM, respectively. As shown in the XPS spectra of the three PDMAPS-AMA-modified fiber materials (Figure S12), S 1s and S 2p peaks are both detected, demonstrating the successful grafting of PDMAPS-AMA onto PA layer. The percentages of S element in the PDMAPS-AMA@Nylon, PDMAPS-AMA@PET, and PDMAPS-AMA@SSM were 2.8%, 2.3%, and 3.1%, respectively (Table S2).

These PDMAPS-AMA-modified fiber materials all behave hydrophilic with water CAs of 16−24° and underwater superoleophobic with oil CAs of 152−154° (Figure S13). When the PDMAPS-AMA@PET is fouled by highly viscous crude oil and then immersed in water, crude oil levitates off from its surface spontaneously without leaving any trace, and the PDMAPS-AMA@PET is self-cleaned (Figure 5b). In comparison, both the pristine PET and the PA@ PET cannot be self-cleaned with some oil residues adhered on their surfaces under the same operation (Figure S14). These results demonstrate the excellent antioil-adhesion property of the PDMAPS-AMA@PET and the successful functionalization of the PA coating. Benefiting from the antioil-adhesion property, the PDMAPS-AMA@PET is capable to separate crude oil/water mixture driven only by gravity. When the crude oil/water mixture (V_{oil}/V_{water} = 1:4) is poured on the PDMAPS-AMA@PET, clear water filtrates through, but crude oil is rejected above the PDMAPS-AMA@PET. After one-step separation, oil content in the filtrate is 7.4 ppm, and the separation efficiency is as high as 99.997%. Simultaneously, the PDMAPS-AMA@PET exhibits an ultrahigh water flux of 54000 L m^{-2} h^{-1}. During 10 separation cycles of the crude oil/water mixture, the water flux fluctuates in the range of 54000 ± 9000 L m^{-2} h^{-1}, and the oil content in the filtrate is always lower than 20 ppm (Figure 5b), indicating the good cycling ability of the PDMAPS-AMA@PET.

Another example is to endow the surface antiprotein-adhesion property by grafting the sulfobetaine zwitterionic polymer, PDMAPS, on the PA layer via a "grafting from" method (Figure 5c). First, 2-aminoethyl methacrylate hydrochloride with vinyl bonds and amino groups is pregrafted onto the PA coating under the catalysis of EDC/NHS. Subsequently, sulfobetaine zwitterionic monomers are initiated to grow on the PA coating via the surface-initiated free radical polymerization. The PDMAPS-modified PA@Nylon, PA@PET, and PA@SSM are denoted as PDMAPS@Nylon, PDMAPS@PET, and PDMAPS@SSM, respectively. The S 1s and S 2p peaks are both detected in the XPS spectra of the three PDMAPS modified fiber materials (Figure S15), revealing the successful grafting of the sulfobetaine zwitterionic maromolecules. The percentages of S element in the PDMAPS@Nylon, PDMAPS@PET, and PDMAPS@SSM are 5.0%, 4.8%, and 5.1%, respectively (Table S3). To evaluate the antiprotein-adhesion property, the PDMAPS@PET was immersed in a fluorescent labeled bovine serum albumin (FITC-BSA) solution for 3 h and then characterized via the confocal fluorescence microscopy. The same operations were performed on the PET and the PA@PET as comparisons. As shown in Figure 5c, the pristine PET is seriously adhered by a large quantity of FITC-BSA proteins. The PA@PET exhibits a slightly improved antiprotein-adhesion property, but is still adhered by some FITC-BSA proteins. In contrast, the PDMAPS@PET exhibits an outstanding antiprotein-adhesion property with nearly no FITC-BSA proteins adhered on it.

In summary, we proposed a strategy for constructing an ultrathin and uniform PA coating with a thickness of tens of nanometers and a coverage of ∼100% on various fiber materials via the IP process. The PA coating exhibited outstanding mechanical stability and good resistance to acid and organic solvents. Benefiting from the full coverage feature and inherent robustness, the PA coating can play the role of physical isolation and protect internal fibers from external damage, like acid corrosion. Further functional modification of the PA coating was also successfully achieved by grafting zwitterions onto its carboxyl groups. On this basis, a series of fiber materials with antioil-adhesion and antiprotein-adhesion properties were constructed, simultaneously realizing effective separation of crude oil/water with both ultrahigh efficiency of 99.997% and ultrahigh water flux of 54000 L m^{-2} h^{-1}. Our work utilizes the liquid/liquid IP process to construct surface coatings on fibers for the first time, and offers a generally feasible strategy for generating fiber materials with robust and multifunctional coatings.

■ ASSOCIATED CONTENT

Supporting Information

The Supporting Information is available free of charge at https://pubs.acs.org/doi/10.1021/acsmacrolett.2c00631.

Water contact angles, surface morphology, chemical composition and element distribution of PA coatings (Figures S1−S8). Stability of the PA@Nylon in acid, alkali and organic solvents (Figures S9 and S10). ^{1}H NMR spectrum of the synthesized PDMAPS-AMA copolymer in D_2O (Figure S11). Chemical composition, wettability and underwater anticrude-oil-adhesion property of the functionalized PA coatings (Figures S12−S15). Detailed chemical compositions (Tables S1−S3) (PDF)

■ AUTHOR INFORMATION

Corresponding Authors

Jian Jin − *Innovation Center for Chemical Science, College of Chemistry, Chemical Engineering and Materials Science & Collaborative Innovation Center of Suzhou Nano Science and Technology, Soochow University, Suzhou 215123, P. R. China;* orcid.org/0000-0003-0429-300X; Email: jjin@suda.edu.cn

Yuzhang Zhu − *i-Lab, Suzhou Institute of Nano-Tech and Nano-Bionics, Chinese Academy of Sciences, Suzhou 215123, P. R. China;* orcid.org/0000-0002-7279-2903; Email: yzzhu2011@sinano.ac.cn

https://doi.org/10.1021/acsmacrolett.2c00631
ACS Macro Lett. 2023, 12, 93−100

Authors

Aqiang Wang − *Innovation Center for Chemical Science, College of Chemistry, Chemical Engineering and Materials Science & Collaborative Innovation Center of Suzhou Nano Science and Technology, Soochow University, Suzhou 215123, P. R. China*

Shoujian Gao − *i-Lab, Suzhou Institute of Nano-Tech and Nano-Bionics, Chinese Academy of Sciences, Suzhou 215123, P. R. China*

Complete contact information is available at: https://pubs.acs.org/10.1021/acsmacrolett.2c00631

Author Contributions

The manuscript was written through contributions of all authors. All authors have given approval to the final version of the manuscript. CRediT: **Jian Jin** conceptualization (lead), project administration (lead), supervision (lead), writing-review & editing (supporting); **Aqiang Wang** data curation (lead), formal analysis (lead), methodology (lead), writing-original draft (lead); **Shoujian Gao** formal analysis (supporting), investigation (supporting), writing-original draft (supporting); **Yuzhang Zhu** conceptualization (lead), investigation (supporting), supervision (supporting), writing-review & editing (lead).

Notes

The authors declare no competing financial interest.

■ ACKNOWLEDGMENTS

This work was financially supported by the National Natural Science Foundation of China (21988102, 22105219), the National Key Research and Development Plan (2019YFA0705800), the Key Research and Development Plan of Jiangsu Province (BE2022056), and the Natural Science Foundation of Jiangsu Province (BK20210132).

■ REFERENCES

(1) Peng, X. S.; Jin, J.; Ichinose, I. Mesoporous Separation Membranes of Polymer-Coated Copper Hydroxide Nanostrands. *Adv. Funct. Mater.* **2007**, *17*, 1849−1855.

(2) Gao, S.; Sun, J.; Liu, P.; Zhang, F.; Zhang, W.; Yuan, S.; Li, J.; Jin, J. A Robust Polyionized Hydrogel with an Unprecedented Underwater Anti-Crude-Oil-Adhesion Property. *Adv. Mater.* **2016**, *28*, 5307−5314.

(3) Zeng, X.; Qian, L.; Yuan, X.; Zhou, C.; Li, Z.; Cheng, J.; Xu, S.; Wang, S.; Pi, P.; Wen, X. Inspired by Stenocara Beetles: From Water Collection to High-Efficiency Water-in-Oil Emulsion Separation. *ACS Nano* **2017**, *11*, 760−769.

(4) Huang, Q.; Cai, Y.; Zhang, X.; Liu, J.; Liu, Z.; Li, B.; Wong, H.; Xu, F.; Sheng, L.; Sun, D.; Qin, J.; Luo, Z.; Lu, X. Aligned Graphene Mesh-Supported Double Network Natural Hydrogel Conduit Loaded with Netrin-1 for Peripheral Nerve Regeneration. *ACS Appl. Mater. Interfaces* **2021**, *13*, 112−122.

(5) Jia, C.; Luo, B.; Wang, H.; Bian, Y.; Li, X.; Li, S.; Wang, H. Precise and Arbitrary Deposition of Biomolecules onto Biomimetic Fibrous Matrices for Spatially Controlled Cell Distribution and Functions. *Adv. Mater.* **2017**, *29*, 1701154.

(6) Wu, Y.; Wang, L.; Guo, B.; Ma, P. X. Interwoven Aligned Conductive Nanofiber Yarn/Hydrogel Composite Scaffolds for Engineered 3D Cardiac Anisotropy. *ACS Nano* **2017**, *11*, 5646−5659.

(7) Baughman, R. H.; Cui, C.; Zakhidov, A. A.; Iqbal, Z.; Barisci, J. N.; Spinks, G. M.; Wallace, G. G.; Mazzoldi, A.; De Rossi, D.; Rinzler, A. G.; Jaschinski, O.; Roth, S.; Kertesz, M. Carbon Nanotube Actuators. *Science* **1999**, *284*, 1340−1344.

(8) Li, Z.; Zhang, H.; Zheng, W.; Wang, W.; Huang, H.; Wang, C.; MacDiarmid, A. G.; Wei, Y. Highly Sensitive and Stable Humidity Nanosensors Based on LiCl Doped TiO_2 Electrospun Nanofibers. *J. Am. Chem. Soc.* **2008**, *130*, 5036−5037.

(9) Yang, G.; Kampstra, K. L.; Abidian, M. R. High Performance Conducting Polymer Nanofiber Biosensors for Detection of Biomolecules. *Adv. Mater.* **2014**, *26*, 4954−4960.

(10) Li, Y.; Lee, D.-K.; Kim, J. Y.; Kim, B.; Park, N.-G.; Kim, K.; Shin, J.-H.; Choi, I.-S.; Ko, M. J. Highly Durable and Flexible Dye-Sensitized Solar Cells Fabricated on Plastic Substrates: PVDF-Nanofiber-Reinforced TiO_2 Photoelectrodes. *Energy Environ. Sci.* **2012**, *5*, 8950−8957.

(11) Liu, W.; Song, M.-S.; Kong, B.; Cui, Y. Flexible and Stretchable Energy Storage: Recent Advances and Future Perspectives. *Adv. Mater.* **2017**, *29*, 1603436.

(12) Wang, X.; Gu, Y.; Xiong, Z.; Cui, Z.; Zhang, T. Silk-Molded Flexible, Ultrasensitive, and Highly Stable Electronic Skin for Monitoring Human Physiological Signals. *Adv. Mater.* **2014**, *26*, 1336−1342.

(13) Bao, L.; Li, X. Towards Textile Energy Storage from Cotton T-Shirts. *Adv. Mater.* **2012**, *24*, 3246−3252.

(14) Wu, W.; Bai, S.; Yuan, M.; Qin, Y.; Wang, Z. L.; Jing, T. Lead Zirconate Titanate Nanowire Textile Nanogenerator for Wearable Energy-Harvesting and Self-Powered Devices. *ACS Nano* **2012**, *6*, 6231−6235.

(15) Xiao, R.; Yu, G.; Xu, B. B.; Wang, N.; Liu, X. Fiber Surface/Interfacial Engineering on Wearable Electronics. *Small* **2021**, *17*, 2102903.

(16) Saleem, H.; Trabzon, L.; Kilic, A.; Zaidi, S. J. Recent Advances in Nanofibrous Membranes: Production and Applications in Water Treatment and Desalination. *Desalination* **2020**, *478*, 114178.

(17) Xue, J.; Wu, T.; Dai, Y.; Xia, Y. Electrospinning and Electrospun Nanofibers: Methods, Materials, and Applications. *Chem. Rev.* **2019**, *119*, 5298−5415.

(18) Zeng, W.; Shu, L.; Li, Q.; Chen, S.; Wang, F.; Tao, X.-M. Fiber-Based Wearable Electronics: A Review of Materials, Fabrication, Devices, and Applications. *Adv. Mater.* **2014**, *26*, 5310−5336.

(19) Yue, X.; Li, Z.; Zhang, T.; Yang, D.; Qiu, F. Design and Fabrication of Superwetting Fiber-Based Membranes for Oil/water Separation Applications. *Chem. Eng. J.* **2019**, *364*, 292−309.

(20) Zhou, Z.; Zhang, S.; Cao, Y.; Marelli, B.; Xia, X.; Tao, T. H. Engineering the Future of Silk Materials through Advanced Manufacturing. *Adv. Mater.* **2018**, *30*, 1706983.

(21) Cipitria, A.; Skelton, A.; Dargaville, T. R.; Dalton, P. D.; Hutmacher, D. W. Design, Fabrication and Characterization of PCL Electrospun Scaffolds-A Review. *J. Mater. Chem.* **2011**, *21*, 9419−9453.

(22) Liu, F.; Hashim, N. A.; Liu, Y.; Abed, M. R. M.; Li, K. Progress in the Production and Modification of PVDF Membranes. *J. Membr. Sci.* **2011**, *375*, 1−27.

(23) Zhao, C.; Xue, J.; Ran, F.; Sun, S. Modification of Polyethersulfone Membranes-A Review of Methods. *Prog. Mater. Sci.* **2013**, *58*, 76−150.

(24) Li, S.; Huang, J.; Chen, Z.; Chen, G.; Lai, Y. A Review on Special Wettability Textiles: Theoretical Models, Fabrication Technologies and Multifunctional Applications. *J. Mater. Chem. A* **2017**, *5*, 31−55.

(25) Deng, Y.; Peng, C.; Dai, M.; Lin, D.; Ali, I.; Alhewairini, S. S.; Zheng, X.; Chen, G.; Li, J.; Naz, I. Recent Development of Super-Wettable Materials and Their Applications in Oil-Water Separation. *J. Cleaner Prod.* **2020**, *266*, 121624.

(26) Yong, J.; Chen, F.; Yang, Q.; Huo, J.; Hou, X. Superoleophobic Surfaces. *Chem. Soc. Rev.* **2017**, *46*, 4168−4217.

(27) Li, S.; Xing, T.; Li, Z.; Chen, G. Structure and Properties of Silk Grafted with Acrylate Fluoride Monomers by ATRP. *Appl. Surf. Sci.* **2013**, *268*, 92−97.

(28) Xue, C.-H.; Guo, X.-J.; Ma, J.-Z.; Jia, S.-T. Fabrication of Robust and Antifouling Superhydrophobic Surfaces *via* Surface-Initiated Atom Transfer Radical Polymerization. *ACS Appl. Mater. Interfaces* **2015**, *7*, 8251−8259.

(29) Rasouli, S.; Rezaei, N.; Hamedi, H.; Zendehboudi, S.; Duan, X. Design, Fabrication, and Characterization of a Facile Superhydrophobic and Superoleophilic Mesh-Based Membrane for Selective Oil-Water Separation. *Chem. Eng. Sci.* **2021**, *236*, 116354.
(30) Seto, H.; Kamba, S.; Kondo, T.; Hasegawa, M.; Nashima, S.; Ehara, Y.; Ogawa, Y.; Hoshino, Y.; Miura, Y. Metal Mesh Device Sensor Immobilized with a Trimethoxysilane-Containing Glycopolymer for Label-Free Detection of Proteins and Bacteria. *ACS Appl. Mater. Interfaces* **2014**, *6*, 13234−13241.
(31) Kato, K.; Uchida, E.; Kang, E.-T.; Uyama, Y.; Ikada, Y. Polymer Surface with Graft Chains. *Prog. Polym. Sci.* **2003**, *28*, 209−259.
(32) Tizzotti, M.; Charlot, A.; Fleury, E.; Stenzel, M.; Bernard, J. Modification of Polysaccharides Through Controlled/Living Radical Polymerization Grafting—Towards the Generation of High Performance Hybrids. *Macromol. Rapid Commun.* **2010**, *31*, 1751−1772.
(33) Liu, X.; Jin, X.; Li, L.; Wang, J.; Yang, Y.; Cao, Y.; Wang, W. Air-Permeable, Multifunctional, Dual-Energy-Driven MXene-Decorated Polymeric Textile-Based Wearable Heaters with Exceptional Electrothermal and Photothermal Conversion Performance. *J. Mater. Chem. A* **2020**, *8*, 12526−12537.
(34) Wu, M.; Ma, B.; Pan, T.; Chen, S.; Sun, J. Silver-Nanoparticle-Colored Cotton Fabrics with Tunable Colors and Durable Antibacterial and Self-Healing Superhydrophobic Properties. *Adv. Funct. Mater.* **2016**, *26*, 569−576.
(35) Zhu, S.; Wang, M.; Qiang, Z.; Song, J.; Wang, Y.; Fan, Y.; You, Z.; Liao, Y.; Zhu, M.; Ye, C. Multi-Functional and Highly Conductive Textiles with Ultra-High Durability through 'Green' Fabrication Process. *Chem. Eng. J.* **2021**, *406*, 127140.
(36) Riazi Kermani, F.; Pawliszyn, J. Sorbent Coated Glass Wool Fabric as a Thin Film Microextraction Device. *Anal. Chem.* **2012**, *84*, 8990−8995.
(37) Ye, M.; Jia, J.; Wu, Z.; Qian, C.; Chen, R.; O'Brien, P. G.; Sun, W.; Dong, Y.; Ozin, G. A. Synthesis of Black TiOx Nanoparticles by Mg Reduction of TiO_2 Nanocrystals and Their Application for Solar Water Evaporation. *Adv. Energy Mater.* **2017**, *7*, 1601811.
(38) Wang, X.; Lu, H.; Liu, W.; Guo, M.; Zhang, M. Electrodeposition of Flexible Stainless Steel Mesh Supported ZnO Nanorod Arrays with Enhanced Photocatalytic Performance. *Ceram. Int.* **2017**, *43*, 6460−6466.
(39) Zhang, Y.; Tian, W.; Liu, L.; Cheng, W.; Wang, W.; Liew, K. M.; Wang, B.; Hu, Y. Eco-Friendly Flame Retardant and Electromagnetic Interference Shielding Cotton Fabrics with Multi-Layered Coatings. *Chem. Eng. J.* **2019**, *372*, 1077−1090.
(40) Qiu, X.; Li, Z.; Li, X.; Zhang, Z. Flame Retardant Coatings Prepared Using Layer by Layer Assembly: A review. *Chem. Eng. J.* **2018**, *334*, 108−122.
(41) Tabassian, R.; Oh, J.-H.; Kim, S.; Kim, D.; Ryu, S.; Cho, S.-M.; Koratkar, N.; Oh, I.-K. Graphene-Coated Meshes for Electroactive Flow Control Devices Utilizing Two Antagonistic Functions of Repellency and Permeability. *Nat. Commun.* **2016**, *7*, 13345.
(42) Zhang, F.; Shi, Z.; Chen, L.; Jiang, Y.; Xu, C.; Wu, Z.; Wang, Y.; Peng, C. Porous Superhydrophobic and Superoleophilic Surfaces Prepared by Template Assisted Chemical Vapor Deposition. *Surf. Coat. Technol.* **2017**, *315*, 385−390.
(43) Zhao, Y.; Tang, Y.; Wang, X.; Lin, T. Superhydrophobic Cotton Fabric Fabricated by Electrostatic Assembly of Silica Nanoparticles and Its Remarkable Buoyancy. *Appl. Surf. Sci.* **2010**, *256*, 6736−6742.
(44) Decher, G. Fuzzy Nanoassemblies: Toward Layered Polymeric Multicomposites. *Science* **1997**, *277*, 1232−1237.
(45) Wei, Q.; Haag, R. Universal Polymer Coatings and Their Representative Biomedical Applications. *Mater. Horiz.* **2015**, *2*, 567−577.
(46) Lee, H.; Dellatore, S. M.; Miller, W. M.; Messersmith, P. B. Mussel-Inspired Surface Chemistry for Multifunctional Coatings. *Science* **2007**, *318*, 426−430.
(47) Ryu, J. H.; Messersmith, P. B.; Lee, H. Polydopamine Surface Chemistry: A Decade of Discovery. *ACS Appl. Mater. Interfaces* **2018**, *10*, 7523−7540.
(48) Cao, Y.; Zhang, X.; Tao, L.; Li, K.; Xue, Z.; Feng, L.; Wei, Y. Mussel-Inspired Chemistry and Michael Addition Reaction for Efficient Oil/Water Separation. *ACS Appl. Mater. Interfaces* **2013**, *5*, 4438−4442.
(49) Hu, W.; Lu, S.; Zhang, Z.; Zhu, L.; Wen, Y.; Zhang, T.; Ji, Z. Mussel-Inspired Copolymer-Coated Polypropylene Mesh with Anti-Adhesion Efficiency for Abdominal Wall Defect Repair. *Biomater. Sci.* **2019**, *7*, 1323−1334.
(50) Yang, H.-C.; Liao, K.-J.; Huang, H.; Wu, Q.-Y.; Wan, L.-S.; Xu, Z.-K. Mussel-Inspired Modification of a Polymer Membrane for Ultra-High Water Permeability and Oil-in-Water Emulsion Separation. *J. Mater. Chem. A* **2014**, *2*, 10225−10230.
(51) Zhang, C.; Ou, Y.; Lei, W.-X.; Wan, L.-S.; Ji, J.; Xu, Z.-K. $CuSO_4/H_2O_2$-Induced Rapid Deposition of Polydopamine Coatings with High Uniformity and Enhanced Stability. *Angew. Chem., Int. Ed.* **2016**, *55*, 3054−3057.
(52) Raaijmakers, M. J. T.; Benes, N. E. Current Trends in Interfacial Polymerization Chemistry. *Prog. Polym. Sci.* **2016**, *63*, 86−142.
(53) Song, Y.; Sun, P.; Henry, L. L.; Sun, B. Mechanisms of Structure and Performance Controlled Thin Film Composite Membrane Formation *via* Interfacial Polymerization Process. *J. Membr. Sci.* **2005**, *251*, 67−79.
(54) Park, S.-J.; Choi, W.; Nam, S.-E.; Hong, S.; Lee, J. S.; Lee, J.-H. Fabrication of Polyamide Thin Film Composite Reverse Osmosis Membranes *via* Support-Free Interfacial Polymerization. *J. Membr. Sci.* **2017**, *526*, 52−59.
(55) Yuan, S.; Zhang, G.; Zhu, J.; Mamrol, N.; Liu, S.; Mai, Z.; Van Puyvelde, P.; Van der Bruggen, B. Hydrogel Assisted Interfacial Polymerization for Advanced Nanofiltration Membranes. *J. Mater. Chem. A* **2020**, *8*, 3238−3245.
(56) Karan, S.; Jiang, Z.; Livingston, A. G. Sub-10 nm Polyamide Nanofilms with Ultrafast Solvent Transport for Molecular Separation. *Science* **2015**, *348*, 1347−1351.
(57) Peng, H.; Zhang, W.-H.; Hung, W.-S.; Wang, N.; Sun, J.; Lee, K.-R.; An, Q.-F.; Liu, C.-M.; Zhao, Q. Phosphonium Modification Leads to Ultrapermeable Antibacterial Polyamide Composite Membranes with Unreduced Thickness. *Adv. Mater.* **2020**, *32*, 2001383.
(58) Yang, Z.; Fang, W.; Wang, Z.; Zhang, R.; Zhu, Y.; Jin, J. Dual-Skin Layer Nanofiltration Membranes for Highly Selective Li^+/Mg^{2+} Separation. *J. Membr. Sci.* **2021**, *620*, 118862.
(59) Zhu, W.-P.; Gao, J.; Sun, S.-P.; Zhang, S.; Chung, T.-S. Poly(amidoamine) Dendrimer (PAMAM) Grafted on Thin Film Composite (TFC) Nanofiltration (NF) Hollow Fiber Membranes for Heavy Metal Removal. *J. Membr. Sci.* **2015**, *487*, 117−126.

https://doi.org/10.1021/acsmacrolett.2c00631
ACS Macro Lett. 2023, 12, 93−100